Iron(III)-induced photooxidation of arsenite in the presence of carboxylic acids and phenols as model compounds of natural organic matter

Xingyun Huang, Ying Peng, Jing Xu, Feng Wu, Gilles Mailhot

Iron(III)-induced photooxidation of arsenite in the presence of carboxylic acids and phenols as model compounds of natural organic matter

Xingyun Huang,[1] Ying Peng,[1,2] Jing Xu,[3*] Feng Wu,[1] Gilles Mailhot [4*]

[1] School of Resources and Environmental Science, Wuhan University, Wuhan, 430079, P. R. China

[2] Hubei Academy of Environmental Science, Wuhan, 430072, P. R. China

[3] School of Water Resources and Hydropower Engineering, Wuhan University, Wuhan, 430079, P. R. China

[4] Université Clermont Auvergne, CNRS, SIGMA Clermont, Institut de Chimie de Clermont-Ferrand, F-63000 Clermont–Ferrand, France.

*Corresponding author

E-mail address: jingxu0506@whu.edu.cn (J. Xu), gilles.mailhot@uca.fr (G. Mailhot).

Abstract

Iron species have essential influence on the environmental/geochemical behaviors of arsenic species in water and soil. Colloidal ferric hydroxide (CFH) induces photooxidation of arsenite (As(III)) to arsenate (As(V)) in water at neutral pH through surface complexation and ligand-to-metal charge transfer (LMCT). However, the effect of the co-existing natural organic matter (NOM) on the complexation-photolysis in this process has remained unclear. In the present work, the photooxidation of As(III) induced by CFH was investigated in the presence of various carboxylic acids and polyphenols as simple model compounds of NOM. Two different light sources of ultraviolet A (UVA) (λ_{max} = 365 nm) and ultraviolet B (UVB) (λ_{max} = 313 nm) were used for photooxidation treatment of the experimental ternary system and the control binary system respectively. The obtained results demonstrated that all investigated NOM inhibited the photooxidation of As(III) in the As(III)/CFH system at pH 7. Moreover, the correlation analysis between the pseudo-first order rate constant k_{obs} and various property parameters of NOM showed that the stable constant for the complexation between Fe(III) and NOM ($logK_{Fe-NOM}$) as well as the molecular weight of NOM and the percentages of total acidity of NOM exhibited significant correlations. A simple quantitative structure-activity relationship (QSAR) model was established between k_{obs} and these three parameters utilizing a multiple linear regression method, which can be employed to estimate the photooxidation efficiency of As(III) in the presence of ferric iron and NOM. Thus, the present work contributes to the understanding of the environmental interactions between NOM and iron.

1. Introduction

Arsenic is a toxic substance exhibiting carcinogenic properties. Hence, the pollution of the environment with this element has become the cause for concern (Smedley and Kinniburgh, 2002; Hughes, 2002; Ball, 2005). In natural aqueous environments, arsenic primarily exists in inorganic oxyacid forms, including arsenite (As(III)) and arsenate (As(V)) (Cullen and Reimer, 1989). It is widely known that As(III) is more mobile and displays higher toxicity than As(V). Thus, the process of oxidative conversion of the former to As(V) is of significance.

The adsorption and oxidation of various metals and their oxides, particularly ones of iron, aluminium, and manganese, affect the form and migration of arsenic in the environment (Oscarson et al., 1981). Our previous study investigated the photochemical oxidation of As(III) on nascent colloidal ferric hydroxide (CFH) in aqueous solutions at pH 6, revealing the mechanism of the transformation of As(III) to As(V). The conducted analysis demonstrated that the photochemical oxidation of As(III) in the presence of nascent CFH occurred through an electron transfer from As(III) to Fe(III), induced by absorption of radiation into the ligand-to-metal charge-transfer (LMCT) band (Xu et al., 2014). Nonetheless, to date, the environmental photochemical processes of the iron-arsenic complexes have not been extensively investigated. This is a consequence of insufficient research into the influence of NOM prevalent in natural waters on the iron-arsenic interaction as well as on the photochemical oxidation processes.

In natural waters, NOM is a mixture of substances formed through the breakdown

72 of plant and animal tissues by biological and chemical processes (Ma et al., 2001). It

73 has been demonstrated that the main functional groups of the NOM components

74 include carboxylic, carbonyl, phenol, and catechol moieties. Evidence also suggests

75 that both As(V) and As(III) can bind to NOM (Thanabalasingam and Pickering, 1986;

76 Liu and Cai, 2010). Notably, the complexation of arsenic with NOM plays an

77 important role in regulating the mobility and transformation of this element in the

78 aquatic environment (Buschmann et al., 2006). Furthermore, interactions with natural

79 organic acids are known to modify the stability and surface reactivity of iron

80 hydroxides (Cheng et al., 2019). Consequently, in view of the high concentrations of

81 iron in natural systems in comparison to those of trace metals, competitive binding of

82 iron to NOM may affect the binding, and thus the fate of other metals.

83 However, as NOM possesses various active functional groups and exhibits large

84 molecular weight, studies involving these substances are often problematic. In many

85 cases, model compounds, such as low molecular weight aliphatic acids, have been

86 employed to simulate the behaviors and/or mechanisms of NOM (Yost et al., 1990;

87 Boily and Fein, 2000; Giannakopoulos et al., 2005). Some of these acids serve as

88 metabolic intermediates in the citric acid and glyoxylate cycles of plants. Examples of

89 such compounds include citric, succinic, fumaric, and malic acids. In addition to the

90 acids, which are continuously being recycled in plants by different metabolic

91 processes, other low molecular weight acids, such as the end products of metabolic

92 pathways of plants, are also known. Examples of these include lactic and oxalic

93 (Wershaw, 2019). And Fe(III)-oxalate is a representative model Fe(III) complex and

94 often used in the study of iron complexes (Zuo, 1995; Chen et al., 2013). Moreover,

95 gallic acid is produced in plants by a degradation reaction and contains a number of

96 hydroxyl (-OH) moieties. Recent investigations demonstrated that at pH ~ 8 (natural

97 seawater pH), the compound is deprotonated, which results in the formation of

4

98　anionic ligands capable of complexing to metals, as the organic ligands at the cell

99　surface of microorganisms (González et al., 2014; López et al., 2015;

100　Santana-Casiano et al., 2010). Polyphenols were included in the present study,

101　because compounds containing hydroxyl and carboxyl functionalities have been

102　shown to complex to Fe(III) (González et al., 2019). The catechol is an organic

103　functional compound. It can form stable complexes with various divalent and trivalent

104　metal ions, among which trivalent ion complexes are the most stable. Depending on

105　the pH value, many mono-, di-, or tri-coordinated complexes can be formed. Among

106　them, the monocoordinated complexes are formed preferentially in a higher

107　proportion. Fe(III) can react with catechol to form a complex to produce Fe(II) and

108　semiquinone radicals. This is a pH-dependent process, which is related to changes in

109　the Fe(III)/Fe(II) redox potential and effective composite stability (Santana-Casiano et

110　al., 2014). Catechol and iron complexes also prevent metals from undergoing redox

111　reactions, as in the case of dicoordinated iron(III) complexes. In contrast,

112　monocoordination complexes allow iron to participate in the electron transfer reaction.

113　This experiment mainly assumes that the ligand form is mainly a single ligand for

114　simulation calculation (Santana-Casiano et al., 2010). NOM possessing carboxylic

115　acids and/or polyphenols is suspected to affect the photooxidation of As(III) on the

116　surface of CFH. However, the structure-activity relationship between these model

117　compounds of NOM and their influence on the photochemical reactivity of the

118　As(III)-CFH complexes remain ambiguous. Buschmann et al.(2005)reported

119　Suwannee River humic acid as the typical dissolved natural organic matter (DOM)

120　induced As(III) photooxidation under UV-A and visible light from a medium-pressure

121　mercury lamp. For 5 mg L^{-1} of dissolved organic carbon (DOC) and 60 mW cm^{-2}

122　UV-A irradiation (366 nm), the rate coefficient k_{exp} was 1.27×10^{-2} min^{-1} (250

123　nM/100 min initial rate was ca. 5.08×10^{-3} μM min^{-1}). Such rate is negligible in our

124　system. And they also fail to study the transformation mechanism of As(III) from the

125　interaction of arsenic, iron and NOM. In fact, in addition to the adsorption of

126　inorganic arsenic on the surface of iron (hydrogen) oxide forms an internal phase

127   complex between surface functional groups and arsenic. Arsenic and iron can also

128   complex with humus substance. Furthermore, interactions with natural organic acids

129   are known to modify the stability and surface reactivity of iron hydroxides. Moreover,

130   in view of the high concentration of iron in natural systems, compared to those of

131   trace metals, competitive binding of iron onto HS may affect the binding, and then the

132   fate, of other metals.

133   Thus, in the present study, we investigated the effect of NOM on the photochemical

134   oxidation process of As(III) in a As(III)/CFH system. Eleven widely-known

135   compounds containing at least two active functional groups (bicarboxylic acids,

136   hydroxyl carboxylic acids, hydroxyl aromatic carboxylic acids, polycarboxylic acids,

137   and polyphenols) were employed as the model compounds of NOM in the

138   environment. A simple quantitative structure-activity relationship (QSAR) model was

139   used to determine the correlation between the properties of NOM and the observed

140   rate constant (k_{obs}). Additionally, the principal structure/property parameters, which

141   impacted the activity of NOM, influencing the photolysis of As(III)-CFH, were

142   determined. Considering that the photochemical processes may differ with the

143   irradiation wavelength, UVA ($\lambda_{max} = 365$ nm) and UVB ($\lambda_{max} = 313$ nm) lamps were

144   utilized as light sources. The present study contributes to the understanding of the

145   sunlight-driven geochemical cycle as well as the fate of arsenic in environments

146   containing NOM and iron.

147

148   **2. Materials and methods**

149   **2.1. Chemicals**

150   Sodium arsenite NaAsO$_2$ (99.5%) was obtained from Xiya Reagent Center (Chengdu,

151   China) and was used after 24 h of drying in a desiccator. Sodium arsenate

152   Na$_2$HAsO$_4$·7H$_2$O (98%) was provided by Alfa Aesar Chemical Co., Ltd. (Tianjin,

153   China). Fe$_2$(SO$_4$)$_3$ (analytical reagent (AR) grade) was purchased from Guangdong

154 Taishan Chemical Co., Ltd. and was employed as the iron source. *Cis*-butenedioic

155 acid (AR), lactic acid (AR), butanedioic acid (AR), ethanedioic acid dihydrate (AR),

156 citric acid monohydrate (AR), salicylic acid (AR), ethylenediaminetetraacetic acid

157 (AR), NaOH (AR), H_2SO_4 (AR), HCl (AR), KOH (AR), $NaH_2PO_4 \cdot 2H_2O$ (AR), and

158 $Na_2HPO_4 \cdot 12H_2O$ (AR) were purchased from Sinopharm Chemical Reagent Co., Ltd.

159 (Shanghai, China). L-(-)-Malic acid (98%), gallic acid (99%),

160 4-nitrocatechol(>98.0%), and catechol (99.0%) were provided by Aladdin Industrial

161 Corporation (Shanghai, China). 1,4-Piperazinediethanesulfonic acid (PIPES, 99.5%)

162 was obtained from Aladdin Biochemical Technology Co., Ltd. (Shanghai, China).

163 KBH_4 (≥97.0%) was purchased from Shanghai Lingfeng Chemical Reagent Co., Ltd.

164 The property parameters of model compounds of NOM used in this study are listed

165 in Table S1 (Supplementary material). Gallic acid and catechol (configured with

166 cooled boiling water) were reconfigured upon each use. All solutions were prepared

167 using deionized water with resistivity of 18.2 MΩ cm obtained from a water

168 purification system (Youpu Ultra Pure Technology Co., Ltd., Sichuan, China). All of

169 the prepared solutions were stored at 4°C and protected from light.

170 **2.2. Photochemical reaction**

171 The emission spectra of the UVA or UVB lamps as the light sources used in the

172 photoreaction experiment, and the schematic of the photoreactor are illustrated in Fig.

173 S1a and 1b (Supplementary material), respectively. The emission spectra ranges were

174 340–400 nm and 290–360 nm with wavelengths of 365 nm and 311 nm,

175 correspondingly. The intensities of the emitted light were 5.5 mW cm^{-2} and 11.8 mW

7

176 cm^{-2}, for UVA and UVB lamps respectively (measure the intensity of light after

177 passing through the reactor wall and circulating water layer inside the reactor). As

178 illustrated in Fig. S1b, the center of the protective sleeve consisted of a cylindrical

179 plexiglass water-jacketed reactor with cooling circulation. A magnetic stirrer was

180 placed under the reactor. Around the reactor, a quadrilateral light source cover was

181 installed, which involved a symmetrical number of UVA lamps on each side of the

182 inner wall. Moreover, ten UVA or UVB lamps (8 W) used for irradiation were placed

183 symmetrically around the reactor.

184 The reaction solutions containing Fe(III), As(III), PIPES, and NOM, as well as ones

185 without NOM, were transferred into a 500 mL reactor. The reaction temperature was

186 set to 25°C and maintained using a circulating water unit. The

187 piperazine-N,N'-bis(2-ethanesulfonic acid) (PIPES) buffer was utilized to maintain the

188 pH at 7.0 ± 0.1. Subsequently, the lamps were switched on and the extent of the As(III)

189 oxidation was evaluated by collecting 4.5 mL samples at fixed interval times. The

190 samples were quenched with 0.5 mL of 1:1 (v/v) HCl/water prior to conducting the

191 tests. All experiments were conducted on solutions that had been exposed to the

192 atmosphere. It is noteworthy that all experiments were repeated 2–3 times, and the

193 variations between experiments are shown by error bars.

194 **2.3. Analysis**

195 The reactions were analyzed by liquid chromatography-hydride generation-atomic

196 fluorescence spectrometry (LC-HG-AFS; Bohui Instrument Co., Ltd., Beijing, China)

197 using a 5% HCl-2% KBH$_4$ solution. Argon (99.99%) was used as a carrier and

198 shielding gas during the analysis. The concentrations of As(III) and As(V) were

199 determined and the observed rate of As(III) oxidation (k_{obs}) was calculated based on

200 the pseudo-first order kinetics using equation (1). The time period of 0-20 min was

201 selected for the calculation of k_{obs}. The k_{obs} value was set as the activity parameter,

202 with which the simple linear fitting and multivariate correlation analyses were

203 conducted to obtain the chemical property parameters of NOM. The correlation

204 analysis was performed by employing the Origin 9.0 software. The values of k_{obs}

205 established under UVA and UVB irradiation were denoted as $k_{obs\text{-}UVA}$ and $k_{obs\text{-}UVB}$,

206 respectively.

$$-\ln(C/C_0) = k_{obs} \times t \#(1)$$

207 where t is the reaction time, C_0 and C are the initial concentration of As (III) and the

208 concentration at any time t in the reaction, and k_{obs} is the initial apparent rate constant

209 of the quasi first-order equation. The ultraviolet-visible (UV-Vis) absorption spectra

210 of the solutions containing Fe(III)-As(III) mixtures were recorded in a 1 cm quartz

211 cuvette using a Shimadzu UV-1601 spectrophotometer (Kyoto, Japan).

212

213 **3. Results and discussion**

214 **3.1. Photochemical oxidation of As(III) in the presence of Fe(III) and various**

215 **NOM**

216 The results of As(III) photooxidation in systems containing various NOM as well as

217 in the control systems (As(III) alone and Fe(III) + As(III) without NOM) under UVA

218 and UVB irradiation are shown in Fig. 1 and 2. Moreover, the experimental values of

219    $k_{obs\text{-}UVA}$ and $k_{obs\text{-}UVB}$ are listed in Table S2. The pH was set to pH 7 for all investigated

220   systems, as it is an average pH of natural waters and the efficiency of photochemical

221   oxidation of As(III) induced by CFH at pH 7 was high. As shown in Fig. 1 and 2, the

222   observed rate constants $k_{\text{obs-}UVA}$ and $k_{\text{obs-}UVB}$ for 5 μM As(III) in the presence of 66 μM

223   Fe(III) were determined at 0.045 min^{-1} and 0.127 min^{-1}, respectively. The two k_{obs}

224   values were used as the corresponding baselines to evaluate the effects of NOM in

225   photochemical systems under UVA and UVB irradiation, respectively. Moreover, the

226   curves for the control system, abbreviated as Fe + As, are presented in all panels in

227   Fig. 1 and 2. It was established that compared with the fast As(III) photooxidation in

228   the presence of CFH, no reaction occurred in the absence of Fe(III) under UVA or

229   UVB irradiation. This outcome is in accordance with our previous report (Xu et al.,

230   2014).

231
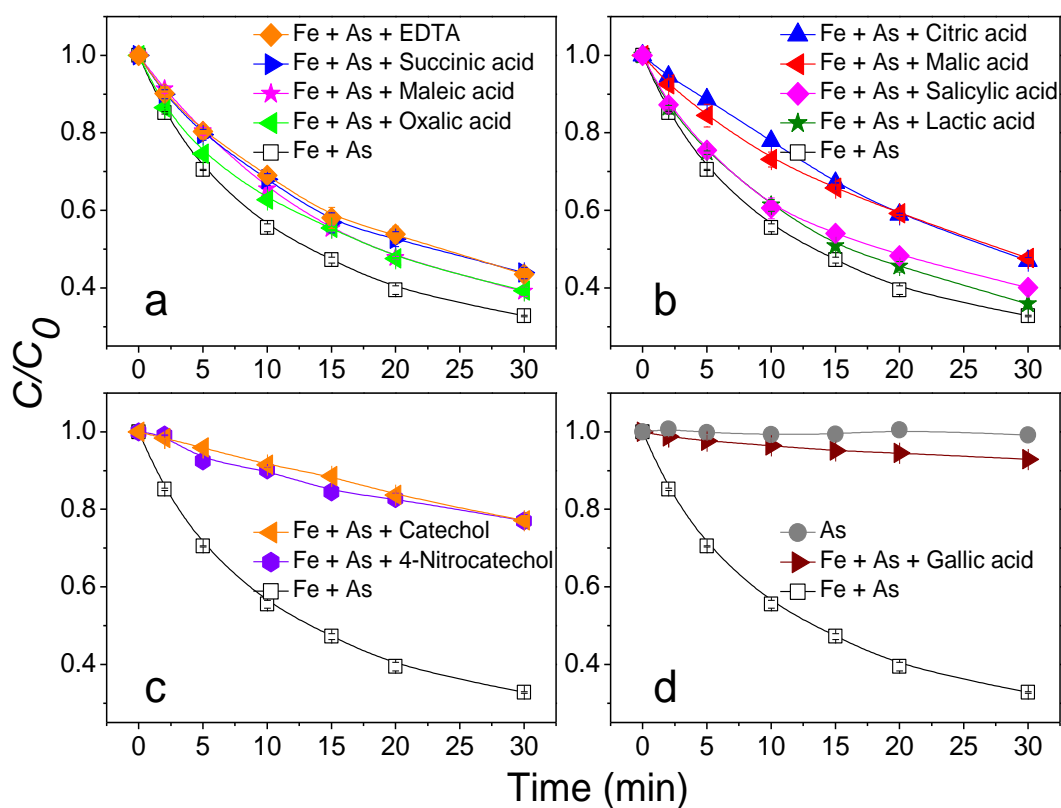
Fig. 1. Effects of different NOM on the photooxidation of As(III) in the presence of Fe(III) under

UVA light source. Initial conditions: [Fe(III)] = 66 μM, [As(III)] = 5 μM, [NOM] = 10 μM,

[PIPES] = 5 mM, pH = 7.

Fig. 1 and 2 show that the addition of 10 μM of each NOM under UVA and UVB irradiation inhibited the oxidation of As(III) to varying degrees. The main reason for this observation is thought to be competitive complexation(Catrouillet et al., 2016). NOM exhibit stronger complexing ability than the As(III) oxyanion; therefore, the investigated compounds inhibited the photochemical oxidation of As(III) via the Fe(III)-As(III) complex. In this case, NOM prevented the surface complexation of the As(III) oxyanion onto CFH at neutral pH and cut-off the pathway of LMCT. It has previously been shown that in ternary systems with metals, e.g. NOM and adsorbent (mineral), NOM can bind directly on the oxide surface, causing blockage of the sites and reduction of the adsorption efficiency (Lai et al., 2002; Fakour et al., 2016). Wang et al. (2013) reported that As(III) was not measurably oxidized in the presence of

11

248 excess EDTA (i.e. Fe(II):EDTA < 1:1), contrasting with the rapid oxidation of Fe(II)

249 by O_2 and H_2O_2 at neutral pH under the same conditions. However, partial oxidation

250 of As(III) was observed at a 2:1 ratio of Fe(II):EDTA. Rapid Fe(II) oxidation in the

251 presence of organic ligands did not necessarily result in the coupled As(III) oxidation.

252 As such, formation of reactive oxidants via iron-catalyzed reactions drives As(III)

253 oxidation and organic ligands regulate the extent and rate of As(III) oxidation by

254 manipulating iron speciation, nature and concentrations of Fenton oxidants. In this

255 study, it is proposed that EDTA competes with As(III) to coordinate with Fe(III), and

256 the formation of Fe(III)-As(III) complexes is gradually reduced in this process, which

257 can also indicate that excessive EDTA completely inhibits oxidation of As(III) under

258 neutral conditions. Consequently, the complexing functional groups in NOM are the

259 predominant features affecting the oxidation rate of As(III).

260
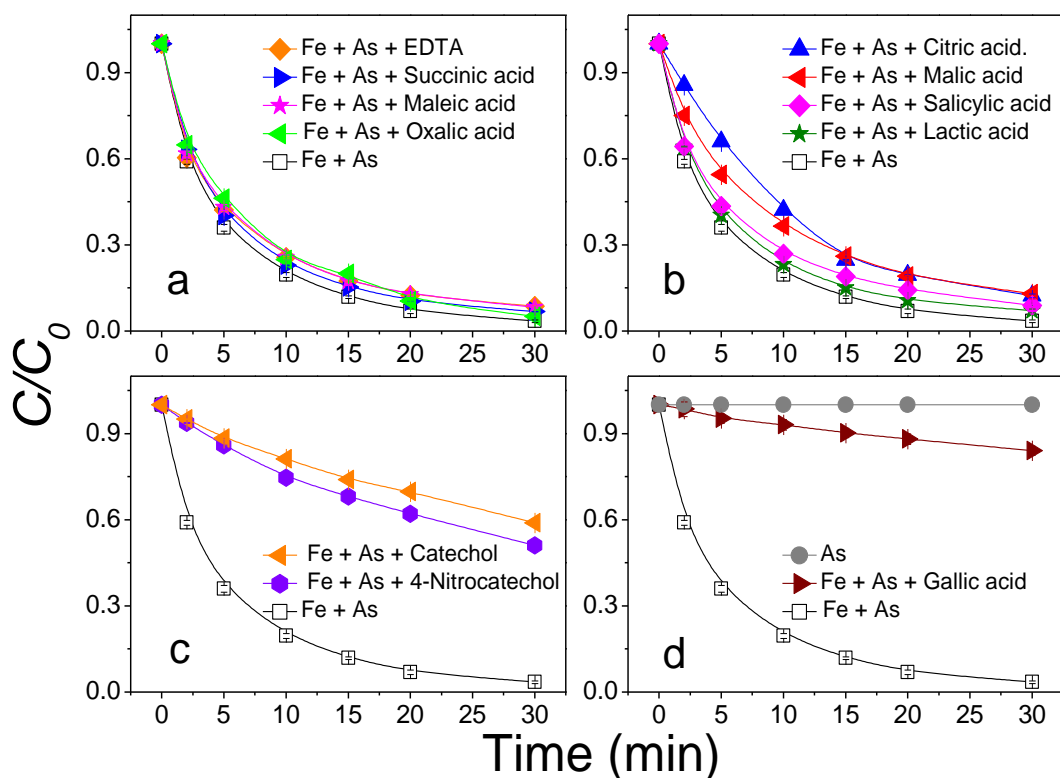
261

262 Fig. 2. Effects of different NOM on the photooxidation of As(III) in the presence of Fe(III) under

263 UVB light source. Initial conditions: [Fe(III)] = 66 μM, [As(III)] = 5 μM, [NOM] = 10 μM,

264 [PIPES] = 5 mM, pH = 7.

265

Based on the data presented in Fig. 1 and Table S2, the values of $k_{\text{obs-}UVA}$ in the

presence of various NOM were determined and classified into three groups. The first

group (group I), with $k_{\text{obs-}UVA}$ of 0.026–0.039 min^{-1} (relative standard deviation, RSD

15%), included lactic, maleic, salicylic, oxalic, succinic, citric, and malic acids as well

as EDTA (Figs. 1a and 1b). Moreover, the second group (group II) with $k_{\text{obs-}UVA}$

established at 0.0087–0.0099 min^{-1} (RSD 9%) included 4-nitrocatechol and catechol

(Fig. 1c). Lastly, the third group (group III), with a $k_{\text{obs-}UVA}$ value of 0.0028 min^{-1},

involved gallic acid (Fig. 1d). The relative minimum inter-group variances of $k_{\text{obs-}UVA}$

between each group were determined at 62% (between group I and II) and 68%

(between group II and III). Analogously, the values of $k_{\text{obs-}UVB}$ in the presence of

various NOM were also classified into three groups. The value of $k_{\text{obs-}UVB}$ for the first

group was determined at 0.081–0.109 min^{-1} (Fig. 2a and 2b, RSD 10%), while for the

second group it was 0.018–0.024 min^{-1} (Fig. 2c, RSD 20%). Additionally $k_{\text{obs-}UVB}$ for

the third group was established at 0.0062 min^{-1} (Fig. 2d). The relative inter-group

minimum variances of $k_{\text{obs-}UVB}$ between each group were 70% (between group I and II)

and 66% (between group II and III). The classification of the NOM into 3 groups

based on the value of k_{obs} was valid, since the relative minimum intergroup variance

was sufficiently large (>3RSD of intragroup data, Table S2) for measurements under

UVA and UVB irradiation.

Overall, the classification in terms of k_{obs} correlates with the present functional

groups. Group I includes polycarboxylic acids (Figs. 1a and 2a) or hydroxyl

13

287　carboxylic acids (Fig. 1b and 2b), group II contains polyphenols without carboxyl

288　moieties (Fig. 1c and 2c), while group III consists of carboxylic polyphenols (Fig. 1d

289　and 2d). However, such classification is not sufficiently precise, particularly for NOM

290　in group I. For instance, polycarboxylic acids and hydroxyl carboxylic acids exhibit

291　similar k_{obs} values; however, the order of these carboxylic acids in terms of k_{obs} is

292　mixed and dissimilar under UVA and UVB irradiation. It was not possible to classify

293　the compounds in group I into two subgroups according to the number of hydroxyl

294　and carboxyl functionalities. Additionally, salicylic acid is an aromatic carboxylic acid,

295　but it is more similar to other carboxylic acids rather than to polyphenols or gallic

296　acid. This implies that the mono-aromatic ring is not a significant structural property

297　of the investigated NOM.

298

299　**3.2. Effects of the wavelength bands of the light sources**

300　The $k_{obs\text{-}UVB}$ value is noticeably larger than the corresponding $k_{obs\text{-}UVA}$ value for each

301　evaluated NOM. Analogous results were obtained for the system without NOM,

302　where the ratio of $k_{obs\text{-}UVB}/k_{obs\text{-}UVA}$ was established at 2.82. The quantum yields of the

303　photolysis of the Fe(III)-As(III) complex were estimated to be close ($\emptyset_{UVB}/\emptyset_{UVA}$= 1.4,

304　Text S1 and Fig. S2). Hence, the difference between $k_{obs\text{-}UVB}$ and $k_{obs\text{-}UVA}$ in the

305　absence of NOM can be attributed to the intensity of the radiation and its absorption

306　by the Fe(III)-As(III) complex, which is not wavelength-dependent. Additionally, to

307　confirm whether the effect of the NOM structure on k_{obs} is dependent on the

308　wavelength, the correlation analysis between $k_{obs\text{-}UVA}$ and $k_{obs\text{-}UVB}$ in the presence of

309 NOM was carried out, as shown in Fig. 3. Linear fitting analysis demonstrated that

310 both in the presence and in the absence of NOM, $k_{obs\text{-}UVB}$ was approximately three

311 times higher than $k_{obs\text{-}UVA}$, and the correlation was significant (r = 0.996, p < 0.001).

312 This result confirmed the hypothesis that the effect of NOM at low concentrations is

313 not dependent on the wavelength band of UVB and UVA, but on the structure.
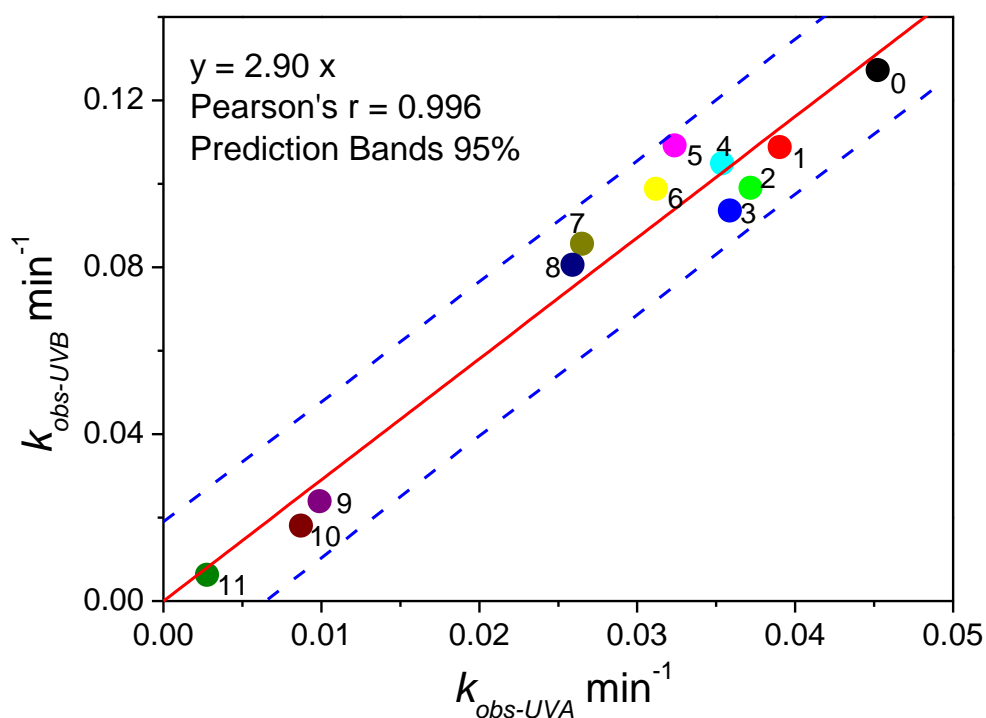
314

315 Fig. 3. Comparative analysis of k_{obs} under UVA and UVB light sources in the presence and

316 absence of NOM. The number 0 represents k_{obs} without NOM, and 1-11 represent k_{obs} with various

317 NOM (1: lactic acid, 2: maleic acid, 3: salicylic acid, 4: oxalic acid, 5: succinic acid, 6: EDTA, 7:

318 citric acid, 8: malic acid, 9: 4-nitrocatechol, 10: catechol, and 11: gallic acid).

319

320 **3.3. Relationship between the property parameters of NOM and k_{obs}**

321 The relationships between k_{obs} and various NOM property parameters were examined

322 to determine the key properties of NOM, which inhibit the oxidation of As(III) in the

323   presence of CFH. The chemical composition properties of the NOM investigated in

324   this study were simply linearly fitted with the values of k_{obs}. The results of the

325   Pearson's correlation carried out to examine the relationships between the variables

326   are shown in Table 1. No significant correlation was observed between k_{obs} and the

327   elemental composition of NOM (C%, H%, or O%, $p > 0.05$). Notably, the parameters

328   of the molecular weight, number of functional groups, acidic functional groups, and

329   pKa (the negative logarithm of the overall acidity constant for the overall ionization

330   reaction of the polyprotic acid) exhibited significant correlation ($p < 0.05$ or 0.01).

331   Most importantly, the correlations between $k_{obs-UVA}$ or $k_{obs-UVB}$ and $logK_{Fe-NOM}$ or pKa_1

332   (the negative logarithm of the acidity constants for the first stage in which a

333   polyprotic acid loses a proton) of NOM were exceptionally significant ($p < 0.001$) and

334   the linear fit curves are presented in Fig. S3. The value of k_{obs} displayed a significant

335   negative correlation with $logK_{Fe-NOM}$, which confirmed that NOM inhibited the

336   oxidation of As(III) by destroying the Fe(III)-As(III) complexes. Therefore, the

337   number/type of functional groups as well as the ionization constant of NOM, which

338   was related to its complexing properties, also exhibited comparatively significant

339   correlation with k_{obs}. Because EDTA and salicylic acid may also form bidentate or

340   tridentate coordination with CFH using the adjacent aromatic carboxyl or phenolic

341   hydroxyl moieties, the values of $logK_{Fe-Sal}$ and $logK_{Fe-EDTA}$ were divided by 2 and 3

342   prior to the correlation analysis, respectively (Fujii et al., 2014). Such treatment of the

343   obtained data resulted in a more significant correlation.

344

345

346

347

348

349

350   Table 1

351   Correlation coefficients between k_{obs} with the property parameters of NOM (***$p < 0.001$, **$p <$

352   0.01, *$p < 0.05$ and p = Pearson correlation coefficient).

k_{obs}	Molecular weight	elemental composition (%)			Number of functional groups	
		C	H	O	N_{COOH}	$N_{OH \text{ or } NH2}$
$k_{obs-UVA}$	-0.647*	-0.445	0.185	0.466	0.501	-0.805**
$k_{obs-UVB}$	-0.672*	-0.542	0.202	0.544	0.617*	-0.806**

	acidic functional groups (%)			logK$_{Fe-NOM}$	pKa$_1$	pKa
	Carboxyl	Hydroxyl	total acidity			
$k_{obs-UVA}$	0.731*	-0.786**	0.623*	**-0.967*****	**-0.894*****	-0.606*
$k_{obs-UVB}$	0.807**	**-0.848*****	0.698*	**-0.954*****	**-0.905*****	-0.672*

353

354   **3.4. Multiple correlation between k_{obs} and the property parameters**

355   Prior to the multi-element correlation analysis in terms of QSAR, the correlation

356   analysis between each property of NOM listed in Table S3 was performed to ensure

357   that the multivariate analysis does not include any autocorrelation factors in the same

358   equations. The results presented in Table S3 show that molecular weight (Mw), Total

359   acidity%, N_{COOH}, N_{OH}, logK$_{Fe-NOM}$, and pKa exhibit a significant auto-correlation with

360   at least two other parameters among all the nine parameters linearly correlated with

361   k_{obs} in Table S2. Among the six evaluated parameters, only three, i.e., Mw, Total

362   acidity%, and $\log K_{Fe\text{-}NOM}$, do not show any correlation between each other. Thus, the

363   two parameter and three parameter multiple linear regressions were performed within

364   the six and three parameters, respectively. The results presented in Table 2 indicate

365   that the three-parameter regressions fit the data better than the two parameter

366   regressions under UVA or UVB irradiation. Thus a simple QSAR model of k_{obs} is

367   established with molecular weight, total acidity% and $\log K_{Fe\text{-}NOM}$ concerning the

368   effect of NOM on As(III) photooxidation. The comparison between the experimental

369   and calculated values of k_{obs} utilizing the developed QSAR model is shown in Fig. 4.

370   The solid line represents the fitted curve, while the dotted line marks the 95%

371   confidence prediction interval. As it can be seen, under UVA or UVB irradiation, the

372   correlation coefficients, R^2, of the fitted QSAR model were 0.929 and 0.914,

373   respectively, and all the data were within the 95% prediction interval. It is noteworthy

374   that the $\log K_{Fe\text{-}NOM}$ parameter accounted for a large proportion in the fitting formula.

375   This meant that among the chemical properties of NOM, the most important factor

376   affecting k_{obs} was the coordination equilibrium constant between NOM and iron. In

377   addition, some of the two-parameter regressions were also significant, e.g., molecular

378   weight and pKa_1. Thus, these simpler models may also be utilized to estimate k_{obs}

379   when $\log K_{Fe\text{-}NOM}$ data are not available (Fig. S4).

380

381

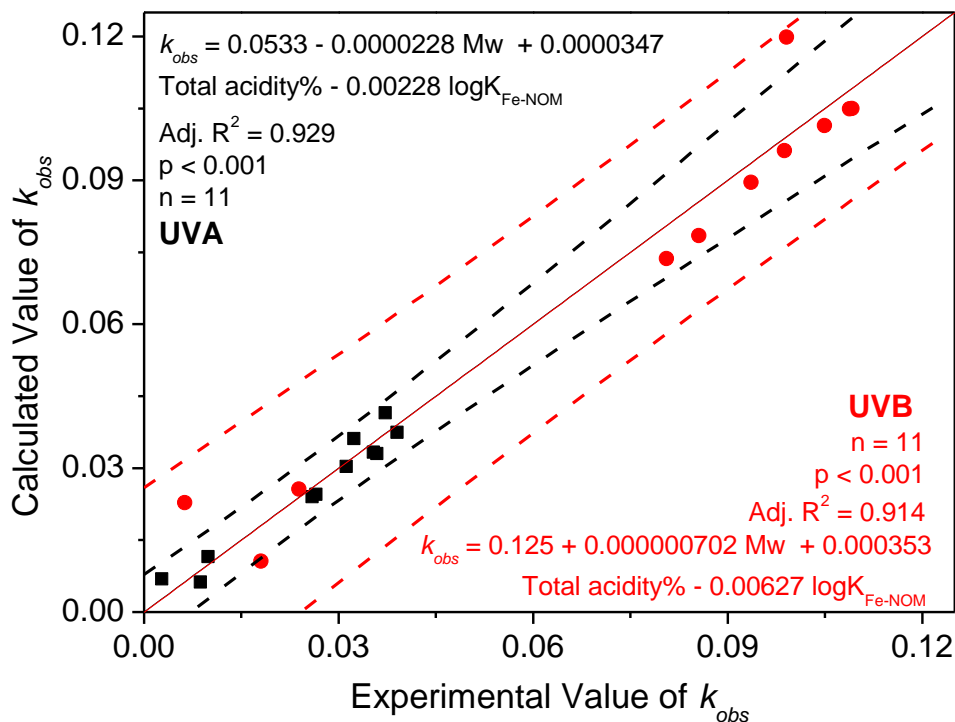382

383

389   Table 2

390   Ternary linear fitting of k_{obs}(UVA and UVB) with property parameters of all NOM evaluated in

391   this study

	No.	Linear Fitting Equation	Adj. R-Square	Residual Sum of Squares	F Value
	(1)	$k_{obs\text{-}UVA}$ **= 0.0527 - 0.0000554 Mw - 0.00432 pKa$_1$**	**0.827*****	**2.28E-04**	**24.9**
	(2)	$k_{obs\text{-}UVA}$ = 0.0318 + 0.00321 N$_{COOH}$ - 0.00943 N$_{OH \, or \, NH2}$	0.665**	4.41E-04	10.9
	(3)	$k_{obs\text{-}UVA}$ = 0.0304 + 0.0000715 Mw - 0.01126 N$_{OH \, or \, NH2}$	0.659**	4.50E-04	10.6
	(4)	$k_{obs\text{-}UVA}$ = 0.0462 - 0.0000632 Mw - 0.000897 OH %	0.622**	4.99E-04	9.21
	(5)	$k_{obs\text{-}UVA}$ = 0.0151 - 0.0000256 Mw + 0.000285 COOH %	0.435*	7.44E-04	4.85
	(6)	$k_{obs\text{-}UVA}$ = 0.0372 + 0.00386 N$_{COOH}$ - 0.00121 pKa	0.441*	7.36E-04	4.95
	(7)	$k_{obs\text{-}UVA}$ = 0.0422 + 0.0000563 Mw - 0.00168 pKa	0.346	8.62E-04	3.64
Binary(1)	(8)	$k_{obs\text{-}UVA}$ = 0.00636 - 0.0000131 Mw + 0.000338 Tot acid %	0.239	1.00E-03	2.57
	(9)	$k_{obs\text{-}UVB}$ **= 0.149 - 0.000112 Mw - 0.0133 pKa$_1$**	**0.808*****	**2.37E-03**	**22.0**
	(10)	$k_{obs\text{-}UVB}$ = 0.0851 + 0.0139 N$_{COOH}$ - 0.0275 N$_{OH \, or \, NH2}$	0.772***	2.82E-03	17.9
	(11)	$k_{obs\text{-}UVB}$ = 0.0805 + 0.000296 Mw - 0.0409 N$_{OH \, or \, NH2}$	0.742**	3.19E-03	15.3
	(12)	$k_{obs\text{-}UVB}$ = 0.132 - 0.000141 Mw - 0.00291 OH %	0.701**	3.69E-03	12.7
	(13)	$k_{obs\text{-}UVB}$ = 0.103 + 0.0157 N$_{COOH}$ - 0.00362 pKa	0.587**	5.10E-03	8.10
	(14)	$k_{obs\text{-}UVB}$ = 0.0283 - 0.0000175 Mw + 0.000970 COOH %	0.566*	5.36E-03	7.51
	(15)	$k_{obs\text{-}UVB}$ = 0.120 + 0.000260 Mw - 0.00569 pKa	0.449*	6.79E-03	5.08
	(16)	$k_{obs\text{-}UVB}$ = - 0.00399 + 0.0000275 Mw + 0.00119 Total acidity %	0.361	7.88E-03	3.82
	(17)	$k_{obs\text{-}UVA}$ = 0.0568 - 0.0000246 Mw - 0.00237 logK$_{Fe\text{-}NOM}$	0.935***	8.63E-05	72.4
	(18)	$k_{obs\text{-}UVA}$ = 0.0491 + 0.0000458 Tot acid % - 0.00226 logK$_{Fe\text{-}NOM}$	0.925***	9.91E-05	62.5
Binary(2)	(19)	$k_{obs\text{-}UVA}$ = 0.0550 - 0.000540 N$_{COOH}$ - 0.00245 logK$_{Fe\text{-}NOM}$	0.921***	1.04E-04	59.6
	(20)	$k_{obs\text{-}UVB}$ = 0.125 + 0.000353 Total acidity % - 0.00627 logK$_{Fe\text{-}NOM}$	0.925***	9.30E-04	62.3
	(21)	$k_{obs\text{-}UVB}$ = 0.145 + 0.0041 N$_{COOH}$ - 0.00667 logK$_{Fe\text{-}NOM}$	0.902***	1.20E-03	47.3
	(22)	$k_{obs\text{-}UVB}$ = 0.161 - 0.0000176 Mw - 0.00719 logK$_{Fe\text{-}NOM}$	0.890***	1.36E-03	41.3
Ternary	**(23)**	$k_{obs\text{-}UVA}$ **= 0.0551 - 0.0000432 Mw + 0.00139 N$_{COOH}$ - 0.00218**	**0.932*****	**7.85E-05**	**46.6**

392

k_{obs} = 0.0533 - 0.0000228 Mw + 0.0000347 Total acidity% - 0.00228 logK$_{Fe-NOM}$

Adj. R^2 = 0.929
p < 0.001
n = 11
UVA

UVB
n = 11
p < 0.001
Adj. R^2 = 0.914
k_{obs} = 0.125 + 0.000000702 Mw + 0.000353 Total acidity% - 0.00627 logK$_{Fe-NOM}$

393

Fig. 4. Comparison of the experimental and theoretical k_{obs} values.

395

4. Conclusion

Employing a panel of various carboxylic acids and polyphenols as the model compounds for NOM, we established that 10 μM of NOM inhibited the photooxidation efficiency of As(III) in the presence of ferric iron in the form of colloidal ferric hydroxide in water at circumneutral pH. This inhibition effect was attributed to the competitive complexation with Fe(III) by NOM vs. As(III), i.e., NOM competes with As(III) to reduce the formation of the Fe(III)-As(III) complex, thereby reducing the rate of the ligand to metal electron transfer during the photolysis and subsequent oxidation of As(III). The described effects were structure-dependent,

405   and the predominant property parameters affecting the process were in the order of

406   $logK_{Fe-NOM}$ > molecular weight > total acidity%. Notably, a simple QSAR equation

407   using these three parameters as the variables was employed to estimate the influence

408   of other NOM not included in this investigation. The present work provides for the

409   first time a valuable reference to understanding the impact of NOM on the

410   interactions between arsenic and iron (hydr)oxides as well as to extending the existing

411   knowledge on the environmental processes of iron species in water. It highlights the

412   important role that organic matter can play on environmental processes and therefore

413   the paramount importance of taking NOM into account in natural processes.

414

419

420

421

422   **References**

423   Ball, P., 2005. Arsenic-free water still a pipedream. Nature 436, 313. https://doi.org/10.1038/436313a.

424   Boily, J.F., Fein, J.B., 2000. Proton binding to humic acids and sorption of Pb(II) and humic acid to the

425   corundum surface. Chem. Geol. 168, 239–253. https://doi.org/10.1016/S0009-2541(00)00197-2.

426   Buschmann, J., Canonica, S., Lindauer, U., Hug, S.J., Sigg, L., 2005. Photoirradiation of dissolved

427   humic acid induces arsenic(III) oxidation. Environ. Sci. Technol. 39, 9541-9546

428   https://doi.org/10.1021/es051597r.

429 Buschmann, J., Kappeler, A., Lindauer, U., Kistler, D., Berg, M., Sigg, L., 2006. Arsenite and arsenate

430   binding to dissolved humic acids: Influence of pH, type of humic acid, and aluminum. Environ.

431   Sci. Technol. 40, 6015–6020. https://doi.org/10.1021/es061057+.

432 Catrouillet, C., Davranche, M., Dia, A., Bouhnik-Le Coz, M., Demangeat, E., Gruau, G., 2016. Does

433   As(III) interact with Fe(II), Fe(III) and organic matter through ternary complexes? J. Colloid

434   Interface Sci. 470, 153–161. https://doi.org/10.1016/j.jcis.2016.02.047.

435 Chen, Y., Zhang, K., Zuo, Y., 2013. Direct and indirect photodegradation of estriol in the presence of

436   humic acid, nitrate and iron complexes in water solutions. Sci. Total Environ. 463–464, 802–809.

437   https://doi.org/10.1016/j.scitotenv.2013.06.026.

438 Cheng, W., Hanna, K., Boily, J.F., 2019. Water Vapor Binding on Organic Matter-Coated Minerals.

439   Environ. Sci. Technol. 53, 1252–1257. https://doi.org/10.1021/acs.est.8b05134.

440 Cullen W, Reimer K, 1989. Arsenic Speciation in the Environment. Chem. Rev. 89(4), 713-764.

441   https://doi.org/10.1021/cr00094a002.

442 Fakour, H., Lin, T.F., Lo, S.L., 2016. Equilibrium Modeling of Arsenic Adsorption in a Ternary

443   Arsenic–Iron Oxide–Natural Organic Matter System. Clean - Soil, Air, Water 44, 1287–1295.

444   https://doi.org/10.1002/clen.201500962.

445 Fujii, M., Imaoka, A., Yoshimura, C., Waite, T.D., 2014. Effects of molecular composition of natural

446   organic matter on ferric iron complexation at circumneutral pH. Environ. Sci. Technol. 48,

447   4414–4424. https://doi.org/10.1021/es405496b.

448 Giannakopoulos, E., Christoforidis, K.C., Tsipis, A., Jerzykiewicz, M., Deligiannakis, Y., 2005.

449   Influence of Pb(II) on the radical properties of humic substances and model compounds. J. Phys.

450   Chem. A 109, 2223–2232. https://doi.org/10.1021/jp045121q.

451   González, A.G., Cadena-Aizaga, M.I., Sarthou, G., González-Dávila, M., Santana-Casiano, J.M., 2019.

452   Iron complexation by phenolic ligands in seawater. Chem. Geol. 511, 380-388.

453   https://doi.org/10.1016/j.chemgeo.2018.10.017.

454   González, A.G., Pokrovsky, O.S., Jiménez-Villacorta, F., Shirokova, L.S., Santana-Casiano, J.M.,

455   González-Dávila, M., Emnova, E.E., 2014. Iron adsorption onto soil and aquatic bacteria: XAS

456   structural study. Chem. Geol. 372, 32-45. https://doi.org/10.1016/j.chemgeo.2014.02.013.

457   Hughes, M.F., 2002. Arsenic toxicity and potential mechanisms of action. Toxicol. Lett. 133, 1-16.

458   https://doi.org/10.1016/s0378-4274(02)00084-x.

459   Lai, C.H., Chen, C.Y., Wei, B.L., Yeh, S.H., 2002. Cadmium adsorption on goethite-coated sand in the

460   presence of humic acid. Water Res. 36, 4943–4950.

461   https://doi.org/10.1016/S0043-1354(02)00009-X.

462   Liu, G., Cai, Y., 2010. Complexation of arsenite with dissolved organic matter: Conditional

463   distribution coefficients and apparent stability constants. Chemosphere 81(7), 890-896.

464   https://doi.org/10.1016/j.chemosphere.

465   López, A., Rico, M., Santana-Casiano, J.M., González, A.G., González-Dávila, M., 2015. Phenolic

466   profile of Dunaliella tertiolecta growing under high levels of copper and iron. Environ. Sci.

467   Pollut. 22, 14820–14828. https://doi.org/10.1007/s11356-015-4717-y.

468   Ma, H., O'Loughlin, E.J., Burris, D.R., 2001. Factors affecting humic-nickel complex mediated

469   reduction of trichloroethene in homogeneous aqueous solution. Environ. Sci. Technol. 35(4),

470   717-724. https://doi.org/10.1021/es001314p.

471   Oscarson, D.W., Huang, P.M., Defosse, C., Herbillon, A., 1981. Oxidative power of Mn(IV) and Fe(III)

472   oxides with respect to As(III) in terrestrial and aquatic environments. Nature 291(5810), 50-51.

473   https://doi.org/10.1038/291050a0.

474   Santana-Casiano, J.M., González-Dávila, M., González, A.G., Millero, F.J., 2010. Fe(III) reduction in

475   the   presence   of   Catechol   in   seawater.   Aquat.   Geochemistry   16,   467–482.

476   https://doi.org/10.1007/s10498-009-9088-x.

477   Santana-Casiano, J.M., González-Dávila, M., González, A.G., Rico, M., López, A., Martel, A., 2014.

478   Characterization of phenolic exudates from Phaeodactylum tricornutum and their effects on the

479   chemistry   of   Fe(II)-Fe(III).   Mar.   Chem.   158,   10–16.

480   https://doi.org/10.1016/j.marchem.2013.11.001.

481   Smedley, P.L., Kinniburgh, D.G., 2002. A review of the source, behaviour and distribution of arsenic

482   in natural waters. Appl. Geochem. 17, 517–568. https://doi.org/10.1016/S0883-2927(02)00018-5.

483   Thanabalasingam, P., Pickering, W.F., 1986. Arsenic Sportion by Humic Acids. Environ. Pollut. Ser. B,

484   Chem. Phys. 12, 233–246. https://doi.org/http://dx.doi.org/10.1016/0143-148X(86)90012-1.

485   Wang, Z., Bush, R.T., Liu, J., 2013. Arsenic(III) and iron(II) co-oxidation by oxygen and hydrogen

486   peroxide: Divergent reactions in the presence of organic ligands. Chemosphere 93, 1936–1941.

487   https://doi.org/10.1016/j.chemosphere.2013.06.076.

488   Wershaw, B.R.L., 2019. Evaluation of Conceptual Models of Natural Organic Matter (Humus) From

489   a   Consideration   of   the   Chemical   and   Biochemical   Processes   of   Humification.   1–58.

490   https://pubs.usgs.gov/sir/2004/5121/.

491   Xu, J., Li, J., Wu, F., Zhang, Y., 2014. Rapid Photooxidation of As(III) through Surface Complexation

492   with   Nascent   Colloidal   Ferric   Hydroxide.   Environ.   Sci.   Technol.   48,   272–278.

493   https://doi.org/10.1021/es403667b.

494   Yost, E.C., Tejedor-tejedor, M.I., Anderson, M.A., 1990. In situ CIR-FTIR characterization of

495   salicylate complexes at the goethite/aqueous solution interface. Environ. Sci. Technol. 24, 0-6.

496   https://doi.org/10.1021/es00076a005.

497   Zuo, Y., 1995. Kinetics of photochemical/chemical cycling of iron coupled with organic substances in

498   cloud and fog droplets. Geochim. Cosmochim. Acta 59, 3123–3130.

499   https://doi.org/10.1016/0016-7037(95)00201-A.

500